doi:10.1093/brain/awu149 Brain 2014: 137; 2231–2244 | 2231

BRAIN
A JOURNAL OF NEUROLOGY

High frequency oscillations are associated with cognitive processing in human recognition memory

Michal T. Kucewicz,[1] Jan Cimbalnik,[1,2] Joseph Y. Matsumoto,[1] Benjamin H. Brinkmann,[1] Mark R. Bower,[1] Vincent Vasoli,[1] Vlastimil Sulc,[1,2] Fred Meyer,[3] W. R. Marsh,[3] S. M. Stead[1] and Gregory A. Worrell[1]

1 Department of Neurology, Mayo Clinic, 200 First St SW, Rochester MN, 55905, USA
2 International Clinical Research Center, St. Anne's University Hospital, Pekarska 53, Brno 656 91, Czech Republic
3 Department of Neurosurgery, Mayo Clinic, 200 First St SW, Rochester MN, 55905, USA

Correspondence to: Gregory Worrell MD, PhD,
Department of Neurology,
Mayo Clinic,
200 First St SW,
Rochester MN, 55905,
USA
E-mail: worrell.gregory@mayo.edu

High frequency oscillations are associated with normal brain function, but also increasingly recognized as potential biomarkers of the epileptogenic brain. Their role in human cognition has been predominantly studied in classical gamma frequencies (30–100 Hz), which reflect neuronal network coordination involved in attention, learning and memory. Invasive brain recordings in animals and humans demonstrate that physiological oscillations extend beyond the gamma frequency range, but their function in human cognitive processing has not been fully elucidated. Here we investigate high frequency oscillations spanning the high gamma (50–125 Hz), ripple (125–250 Hz) and fast ripple (250–500 Hz) frequency bands using intracranial recordings from 12 patients (five males and seven females, age 21–63 years) during memory encoding and recall of a series of affectively charged images. Presentation of the images induced high frequency oscillations in all three studied bands within the primary visual, limbic and higher order cortical regions in a sequence consistent with the visual processing stream. These induced oscillations were detected on individual electrodes localized in the amygdala, hippocampus and specific neocortical areas, revealing discrete oscillations of characteristic frequency, duration and latency from image presentation. Memory encoding and recall significantly modulated the number of induced high gamma, ripple and fast ripple detections in the studied structures, which was greater in the primary sensory areas during the encoding (Wilcoxon rank sum test, $P = 0.002$) and in the higher-order cortical association areas during the recall (Wilcoxon rank sum test, $P = 0.001$) of memorized images. Furthermore, the induced high gamma, ripple and fast ripple responses discriminated the encoded and the affectively charged images. In summary, our results show that high frequency oscillations, spanning a wide range of frequencies, are associated with memory processing and generated along distributed cortical and limbic brain regions. These findings support an important role for fast network synchronization in human cognition and extend our understanding of normal physiological brain activity during memory processing.

Keywords: high frequency oscillations; cognitive processing; memory; gamma oscillations; neural networks

Abbreviation: HFO = high frequency oscillation

Received February 14, 2014. Revised April 14, 2014. Accepted April 15, 2014. Advance Access publication June 11, 2014

Introduction

Direct electrophysiological recordings from the human brain offer a unique opportunity to investigate the neural correlates of our perception, memory and higher brain functions. These cognitive phenomena are thought to be orchestrated by widespread cortical and subcortical neuronal networks, coordinated into synchronous oscillations spanning a wide spectrum of frequencies (Buzsáki, 2006). High frequency oscillations (HFOs) extend beyond the limits of gamma band activity and recently have been the focus of animal and human studies of the neurophysiology of cognition and epilepsy (for a review see Le Van Quyen, 2012). Data collected from multiple intracranial cortical surface and penetrating electrodes provide unique technology for sampling the network activity in the high frequency bands in humans (Worrell *et al*., 2012) and comparing the roles of HFOs in health and disease (Crone *et al*., 2006; Jerbi *et al*., 2009; Lachaux *et al*., 2012).

Studies of HFOs in normal cognition have largely focused on gamma frequencies up to 100 Hz. Initially implicated in synchronizing the activity of neurons encoding sensory features of external stimuli in the cat visual cortex, gamma oscillations were subsequently proposed to subserve a general mechanism for binding coherent object representations in the brain (Singer and Gray, 1995). They are induced in the sensory as well as in the higher order cortical processing areas, driven by bottom–up and top–down mechanisms (Mumford, 1992), respectively, and have been associated with formation of perceptual and memory representations in humans (Tallon-Baudry and Bertrand, 1999; Jensen *et al*., 2007; Tallon-Baudry, 2009). Hence, network oscillations in gamma frequency band and beyond were proposed to coordinate fundamental neuronal processes underlying cognition (Fries, 2009).

Much less is known about the physiological role of HFOs beyond the gamma band. These ultra-fast neuronal oscillations—averaging hundreds of cycles per second—were primarily documented in the rodent hippocampus as part of sharp-wave ripple complexes, known as 'ripples'. Ripples are brief discharges of synchronized firing of neuronal ensembles, mainly occurring during states of rest and sleep (Buzsáki *et al*., 1992). In sleep, ripples have been associated with replay of activity among specific hippocampal neurons that were active during preceding behaviour in rats (Wilson and McNauhgton, 1994; Foster and Wilson, 2006). Ripple activity has been linked to learning and memory consolidation, but recent evidence also suggests an active role in planning (Dragoi and Tonegawa, 2011) and decision-making (Jadhav *et al*., 2012; Singer *et al*., 2013). Whether the human ripple-frequency HFOs support the same function as the hippocampal ripples in rodents remains to be established, as well as their role in the neocortex. At least two studies suggest involvement of rhinal cortical ripples and high gamma oscillations in human memory consolidation (Axmacher *et al*., 2008; Le Van Quyen *et al*., 2010).

Human HFOs of frequencies faster than the ripples, called 'fast ripples' (250–500 Hz), were initially associated with pathological network activity in epilepsy (Bragin *et al*., 1999; Staba *et al*., 2002). Subsequently, interictal gamma (Worrell *et al*., 2004) and ripple (Worrell *et al*., 2008) HFOs were also reported to be increased in the seizure onset zone in patients with focal epilepsy (Worrell and Gotman, 2011). In addition, oscillations in the fast frequency range have been associated with normal physiological functions (Curio, 2000; Baker *et al*., 2003; Barth, 2003; Traub, 2010). Hence, the frequency of a HFO does not seem to distinguish whether it is pathological or physiological. Nonetheless, as HFOs are increased in focal epileptogenic brain, the possibility that they could be used as a clinical biomarker has received considerable interest (Staba, 2010; Engel, 2011; Worrell and Gotman, 2011). Distinguishing between epileptiform HFOs and physiological HFOs involved in cognitive processes remains a challenge (Matsumoto *et al*., 2013*a*). Here we investigated and characterized gamma, ripple and fast ripple HFOs recorded directly from human brain during memory encoding and recall.

Materials and methods

Subjects

Twelve patients (five males and seven females) undergoing intracranial seizure monitoring for surgical treatment of epilepsy agreed to participate in this Mayo Clinic Institutional Review Board approved study (Table 1). Each patient was informed about the study aims by the experimenter and provided with a written consent form for more details. Target locations of the implanted electrodes were determined solely by the clinical requirements, with net unequal distribution of implanted electrodes in the cortical and subcortical structures studied (Supplementary Table 1).

Electrode localization

After surgical implantation patients underwent a high-resolution CT and MRI scan to determine the localization of the electrodes. The scans were fitted to a Talairach brain atlas and the derived coordinates were mapped onto Mayo 3D Brain Atlas (Mayo Clinic) using Analyze software (Analyze Direct Inc.). Data from the electrodes implanted in the limbic and neocortical structures were categorized into six groups: hippocampus, amygdala and parahippocampal, temporal, frontal and occipital neocortex. These six brain structures are consistently colour coded throughout the study: the occipital cortex (red), parahippocampal cortex (orange), hippocampus (green), amygdala (cyan), temporal cortex (blue) and frontal cortex (magenta).

Electrophysiological recordings

Various combinations of penetrating depth electrodes and subdural electrode grids (AD-Tech Inc.) were surgically implanted for prolonged seizure monitoring (Table 1) according to the clinical requirements. Subgaleal or mastoid electrode was used as a recording reference. Data were continuously acquired at 32 kHz from up to 128 channels (Digital Lynx, Neuralynx Inc.) and stored as a custom format for compression and storage (Brinkmann *et al*., 2009).

Visual recognition memory task

Implanted patients were first presented with a set of 80 images from the International Affective Picture Set on a laptop computer screen (Lang *et al*., 1997) and were asked to rate the affective charge of each picture and remember it for subsequent recall 24 h later

Table 1 Details of the intracranial patient recordings

Patient ID	Sex	Age	Clinical condition	Task data	Electrodes	Brain structures	Total implanted electrodes, *n*
1	M	36	TLE	Encoding + recall	Bilateral depth	OC, PH, HP	14
2	F	28	TLE	Encoding + recall	Bilateral depth	OC, PH, HP, AM	14
3	F	21	TLE	Encoding + recall	Left depth and surface	OC, PH, AM, HP, TC	63
4	F	22	TLE	Encoding	Left depth and surface	PH, HP, TC, FC	28
5	F	25	TLE	Encoding + recall	Left depth	PH, HP	9
6	F	34	TLE	Encoding + recall	Bilateral depth	OC, PH, HP	22
7	M	63	TLE	Encoding + recall	Bilateral depth, right surface	OC, HP, FC	50
8	M	40	TLE	Encoding + recall	Bilateral depth, left surface	OC, PH, HP, AM, TC	50
9	M	45	TLE	Recall	Bilateral depth	PH, HP	18
10	F	22	TLE	Encoding + recall	Bilateral depth	OC, PH, HP	14
11	M	44	TLE	Encoding + recall	Bilateral depth	OC, PH, HP, AM	14
12	F	23	TLE, FLE	Encoding + recall	Bilateral depth and surface	HP, AM, TC, FC	132

TLE = intractable temporal lobe epilepsy; FLE = intractable frontal lobe epilepsy; OC = occipital cortex; PH = parahippocampal cortex; HP = hippocampus; AM = amygdala; TC = temporal cortex; FC = frontal cortex.

(Matsumoto *et al*., 2013*b*). In every trial, an image was displayed for 6 s followed by 2 s of blank screen. After that the patient was prompted to rate the picture's affective charge on a 5-point scale, ranging from 'very unpleasant' to 'very pleasant', by pressing a labelled key. The key press initiated an intertrial interval of 6 s preceding the next trial of this encoding stage of the task.

The recall stage of the task was analogous to the encoding, only this time 140 images were presented including the 80 pictures shown 24 h earlier mixed with 60 new pictures not shown previously. Images were presented for 6 s, followed by 2 s of blank screen and then a screen prompt asking the patient to indicate whether the image was 'old' or 'new' by pressing a labelled key. The key press triggered a second question asking the subject to rate their level of certainty on a 3-point scale, which ranged from 'very certain' to 'very uncertain'. The key press initiated the 6 s intertrial interval preceding the next recall trial. The subject's key presses were synchronized with the electrophysiological recordings through a parallel input port using transistor-transistor logic (Digital Lynx, Neuralynx Inc.). The task was run in Presentation software (Neuro behavioral systems Inc.), which additionally logged the time of patient's behavioural responses.

Data preparation

The acquired electrophysiological data, sampled at 32 kHz, were filtered between 0.1–1000 Hz before decimating the data to 5 kHz sampling rate for the analysis of oscillations up to 500 Hz. Bipolar differential signals were derived by differentiating neighbouring electrode pairs to remove any confounds from the common reference signal (Burke *et al*., 2013) including any non-cerebral artefacts. These were minimized by comparing selected data epochs with simultaneous scalp EEG recordings (Ball *et al*., 2009) to identify muscle artefacts associated with grimacing, chewing, ocular movements and microsaccades (Yuval-Greenberg *et al*., 2008; Jerbi *et al*., 2009; Kovach *et al*., 2011). It is critical to remove these artefacts and any epileptiform spikes and sharp transients to prevent false positive HFO detections (Worrell *et al*., 2012). A narrow band filter will also generate spurious oscillations in the vicinity of a sharp transient, but can be differentiated from true oscillation by correlating the filtered and the raw signals. Hence, the bipolar signals were first normalized by their standard deviation (SD) and cut into 18 s segments (from 6 s before to 12 s after image presentation), followed by visual inspection of the raw signal and spectrogram of every single trial epoch. Trials with 60 Hz line noise (increased 60 Hz power in the spectrogram), epileptiform spikes, or muscle artefacts (complex pattern of high-frequency power increase, verified in the scalp EEG recording) were removed from the analysis. Electrodes with >30% of epochs containing epileptiform spikes were excluded from the study (Supplementary Table 1) to minimize the potential confound of epilepsy pathophysiology on the results. Electrodes localized in the clinically diagnosed 'seizure onset zone' were not used in the study at all. In total, 28% (125/444) of all implanted electrodes during the task encoding and 32% (142/444) during the recall stage were used in this study (Supplementary Table 1 and Supplementary Fig. 5).

Data analysis

All analyses were performed in Matlab using custom-made and adapted codes (Mathworks Inc.) and the results are presented as mean ± standard error of the mean (SEM), unless stated otherwise. Time–frequency spectrograms of trial-averaged oscillatory activity were computed with Chronux toolbox for multi-taper Fast Fourier Transform analysis (Chronux, www.chronux.org; see Bokil *et al*., 2010). Multi-taper analysis was used to take advantage of more precise frequency resolution as compared to other methods of spectral analysis (van Vugt *et al*., 2007). Hilbert transform was chosen for precise temporal resolution of significant power changes (see below). The multi-taper method calculates power density with a specified number of tapers, in a moving window of specified frequency and time duration. The taper parameters chosen for the analysis of HFOs were: two tapers, 4 Hz bandwidth, 1 s sliding time window advanced by 100 ms steps [params.tapers = (4 1 6), 1–500 Hz range, no padding]. Error bars of the calculated power were estimated with a Chronux in-built Jackknife function, i.e. resampling the available data sets and estimating confidence intervals at 0.01 significance level. The output spectrogram matrix was log transformed to normalize for the power law differences between the low and high frequencies and was divided by mean power along the frequency axis to obtain power change across the 18 s of the task trial. These time–frequency power change values were collected from all of the electrodes used in the study and mapped onto a universal 3D brain surface by the electrodes'

Talairach coordinates (Freesurfer, www.surfer.nmr.mgh.harvard.edu/) to compare task-induced activity across the different brain structures. Videos were made by taking the average power change value in a given frequency band in 500 ms steps and interpolating the obtained values between the neighbouring recording sites with respect to the 3D brain surface.

Significant increases in the HFO power were detected trial-by-trial using a method based on Hilbert transform applied across independently filtered bands of normalized data segments (Canolty *et al.*, 2006). First, the 18 s data segment (corresponding to one trial) was Butterworth band-pass filtered (third order) for every 1 Hz band step of the 50 to 500 Hz frequency range. Then, the filtered data bands were independently *z*-scored and plotted together on a time–frequency spectrogram (Canolty *et al.*, 2006; Matsumoto *et al.*, 2013*a*, *b*; see Fig. 3). Incidences of significantly increased power were determined by transforming the time–frequency power changes into a binary image thresholded at the *z*-score of 3.0 (ones) and thus separated from subthreshold power fluctuations (zeroes). The 3.0 threshold for significant power increase was set even higher than in a recent report using analogous method for detecting high gamma and ripple events in rats (*z*-score > 2.0 of normalized power) (Sullivan *et al.*, 2011). Only the detections with minimum of one complete cycle above this conservative threshold were included in the analysis to ensure that the detected events are not mere instantaneous power fluctuations but actual oscillations of defined durations (Figs 4C and 5). Duration of each detected HFO event was estimated between two local minima surrounding the detected peak in the power envelope. Peak frequency, onset latency from image presentation and the peak *z*-score amplitude were also determined for every HFO detection. Cumulative plots of the resultant trial-by-trial HFO detections closely overlapped the trial-averaged power changes obtained using the multi-taper analysis method, mutually corroborating the two independently obtained results (Fig. 2). Due to the power change normalization both methods were very sensitive in detecting low-amplitude power changes at the cost of being susceptible to large amplitude power changes associated with epileptiform and non-cerebral artefacts (e.g. epileptiform spikes or sharp-waves). Therefore, the raw signal and spectrogram of each data segment used in the study was individually inspected (see 'Data preparation' section).

Electrodes with significantly increased number of the trial-by-trial HFO detections in response to image presentations were assessed with Kruskal-Wallis non-parametric ANOVA, which tested for the effect of 1 s time bins around the image presentation (five 'baseline' bins before and three bins after) on the number of HFO counts in a given set of trials (Figs 2 and 7B). The bins with significantly increased number of HFO counts per trial were determined using paired non-parametric Wilcoxon signed-rank comparison with their trial-matched average counts from the five baseline bins (Fig. 7) preceding image presentation. Comparison between trials with encoded versus novel and affective versus neutral images was verified using the non-parametric Friedman ANOVA with Bonferroni correction for multiple comparisons. The population properties of induced HFOs (detected from 0–1 s after image presentation on the electrodes that showed significant HFO responses) in different brain structures were tested with unpaired non-parametric Wilcoxon rank sum comparisons summing up all detections from the study. These comparisons included the onset latencies from the image presentation, durations, peak frequencies, amplitude and the trial counts during encoding and recall stages of the task (Figs 4–6). The Kruskal-Wallis test was used to assess the effect of the frequency band on the induced HFO count (normalized by the total number of detections in any one structure) in the first 100 ms following image presentation.

Results

Cognitive processing induces high frequency oscillations in distributed network of cortical and limbic structures

Twelve patients undergoing intracranial EEG monitoring for evaluation of drug resistant epilepsy performed a visual recognition memory task (Table 1) using the International Affective Picture System (Lang *et al.*, 1997). Cognitive processing associated with the encoding and recall of the visual images induced focal increases in high gamma, ripple and fast ripple frequency spectral power (Fig. 1; 27 bipolar electrodes; Supplementary Videos 1–3). This induced high frequency response was found in all of the cortical and limbic structures studied (Fig. 1: temporal cortex; Fig. 2: hippocampus, occipital and parahippocampal cortices; Fig. 3 and Supplementary Fig. 2: prefrontal cortex; Fig. 6: hippocampus; amygdala) using both penetrating depth electrode and subdural grid electrodes, and was observed in 11 of 12 patients studied, in at least two patients for any one structure (Supplementary Fig. 5). In contrast to the multi-focal pattern of power induction in the high frequency bands, low frequency theta/alpha/beta (4–15 Hz) power showed widespread global reduction in response to image presentation. These observations are congruent with the evidence for asynchronous multi-focal gamma oscillations in memory processing, contrasted by synchronous global attenuation of the theta/alpha oscillations (Burke *et al.*, 2013; Supplementary Video 4), in agreement with the general notion of global state modulation by the latter and localized information encoding by the former (Silva, 2013).

Looking more closely at the high frequency band power induction in a trial-by-trial analysis we isolated individual discrete HFO events (Fig. 2) using a Hilbert transform-based method (Fig. 3; see 'Materials and Methods' section). We detected all instances of significant HFO discharges in the 50–500 Hz range (*z*-score > 3.0) and determined their peak frequency, amplitude, duration and latency from the time of image presentation. Picture presentation induced HFOs in high gamma, ripple and fast ripple bands, which closely overlapped with the trial-averaged power changes obtained with a different method of multi-taper spectral analysis (Fig. 2). These discrete HFO detections were observed in the high gamma, ripple and fast ripple frequency ranges in agreement with the trial-averaged multi-taper power changes (Figs 2 and 3), corroborating the Hilbert-transform method detections for quantification of the induced HFO responses. The induced HFO response reached the highest frequencies of ~600 Hz (Supplementary Fig. 2; see Gaona *et al.*, 2011). Each detection had a discrete duration and a signature frequency (Fig. 3; see Supplementary Fig.1 for comparison with a wide-band power increase produced by a sharp transient artefact). HFO detections were binned every 1 s from 5 s before image presentation to 3 s after and their counts were compared across the task trials to isolate electrodes showing significant HFO inductions (Fig. 2; Kruskal-Wallis test, seven bipolar electrodes, $P < 0.01$).

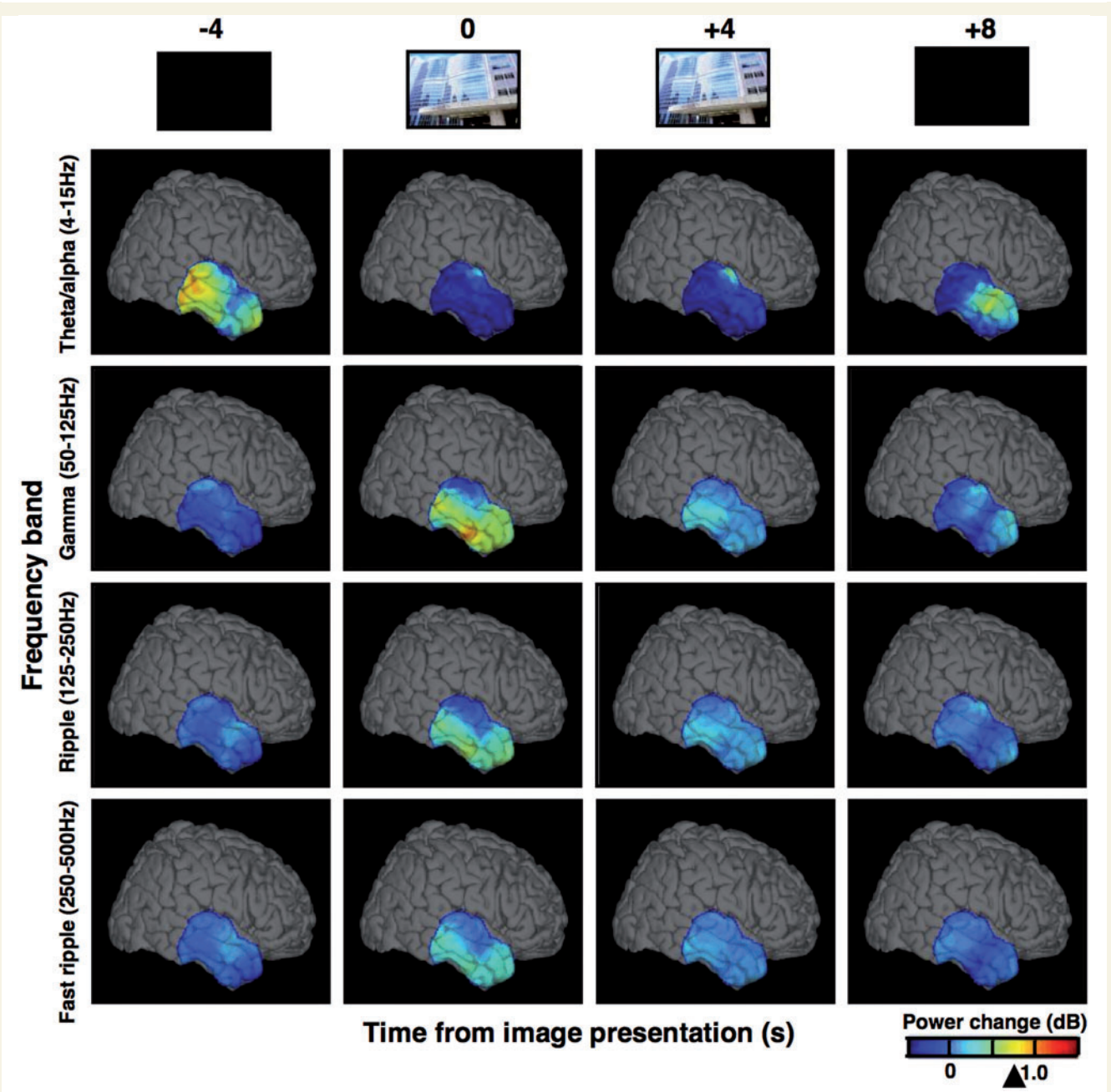

Figure 1 Cognitive processing induces widespread power decrease in low frequency oscillations and focal increases in high frequency bands. The 3D brain views show normalized spectral power changes recorded from temporal cortical surface electrodes (4 × 6 grid) in Patient 8. The power changes are displayed for four frequency bands of oscillations, snapshot at four time-points of trial-averaged image encoding (time 0 corresponds to image presentation). Notice the diffuse loss of low frequency power and emergent multifocal activation in the inferior temporal cortex in all HFO bands, including gamma, ripple and fast ripple frequencies (arrowhead on the power scale points to Jack knifed upper error estimate at $P < 0.01$ significance level). Note, the power values were interpolated between the electrodes of the grid (spaced 1 cm from each other). See Supplementary Videos 1–4 to view these power changes in real-time of the task trials.

Properties of the induced high frequency oscillations parallel the sequence of the visual processing stream

If the induced discrete HFOs reflected processing of the presented images, one would expect them to emerge in a sequence of the theoretical model of the ventral visual stream (Mishkin *et al.*, 1983; Fig. 4A). We found that the number of detections from the electrodes with the significant HFO response (Kruskal-Wallis test, $P < 0.01$; Supplementary Table 1) were first rapidly increased in the occipital cortex (between 100–300 ms after image presentation), then in the parahippocampal cortex (200–500 ms) and

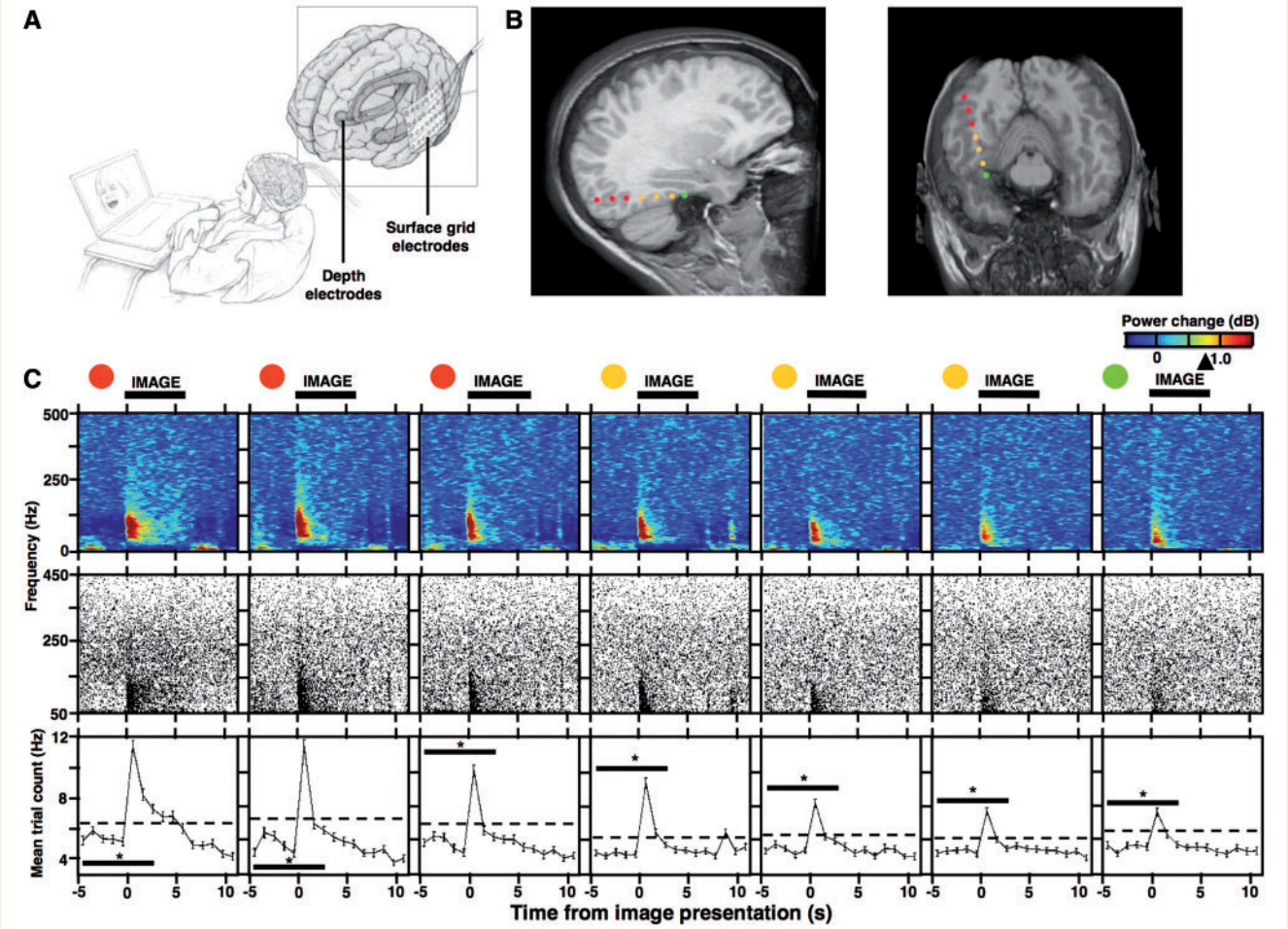

Figure 2 Quantification of cognitively induced HFOs. (**A**) Sketch of the experimental setup for intracranial patient recordings during the visual recognition memory task. (**B**) MRI scans show localization of seven bipolar depth-electrode recording sites (reconstructed from a high resolution CT images of the original eight contact points; see Burke *et al*., 2013) in the right occipital cortex (red), parahippocampal cortex (orange), and the hippocampus (green) from Patient 10. (**C**, *top*) Spectrograms of normalized trial-averaged power changes ($n = 140$ trials; obtained with the multi-taper spectral analysis) were obtained from the seven bipolar recording sites in **B** (colour-coded) during memory encoding (image presentation time indicated by the horizontal black bar; arrowhead on the power scale points to Jackknifed upper error estimate at $P < 0.01$ significance level); (**C**, *middle*) cumulative scatterplots show HFO detections from individual trials (140 trials; detected with the Hilbert spectral analysis method—each black dot is one detection – see Fig. 3 and 'Materials and methods' section for more details) aligned to the time axis of the spectrograms (notice the close overlap between the activation pattern in trial-averaged power spectrograms and the cumulative HFO scatterplots obtained with the multi-taper and Hilbert transform spectral analyses, respectively); (**C**, *bottom*) the HFO detections from the middle panel were summarized as mean trial counts and binned across the same time-axis (dashed line indicates 3 SD above the mean of the five 'baseline' bins preceding the image onset). The mean counts from these five baseline bins and the following three bins that overlapped with image presentation (indicated by black significance bar) were used to quantify significant induction of HFO detections (Kruskal-Wallis test, eight time bins, 140 trials, $^*P < 0.01$). Notice that in this example all of the electrodes from the three structures showed significant inductions of HFO discharges, overlapping with the profile of significant induction in the trial-averaged power spectrograms (see Supplementary Fig. 2 for another example of prefrontal cortical electrode response).

lastly in the hippocampus, amygdala and the temporal and prefrontal cortex (300 ms+; Fig. 4B). Latencies of these induced HFOs were significantly different between the primary visual cortex, i.e. occipital, and the higher associational areas, including parahippocampal, hippocampus, amygdala and temporal and frontal cortices (Wilcoxon rank sum test, $P < 0.01$) and their distribution peaks followed the sequence consistent with the ventral visual processing stream both during the encoding (Fig. 4B) and the recall stages (Supplementary Fig. 3B). This sequential activation pattern was observed in all three HFO frequency bands studied, which showed consistent pattern of high gamma, ripple and fast ripple detection latencies (Fig. 5). These results also agree with the hierarchical processing latencies reported for single-unit activity in the medial temporal lobe structures (Mormann *et al*., 2008).

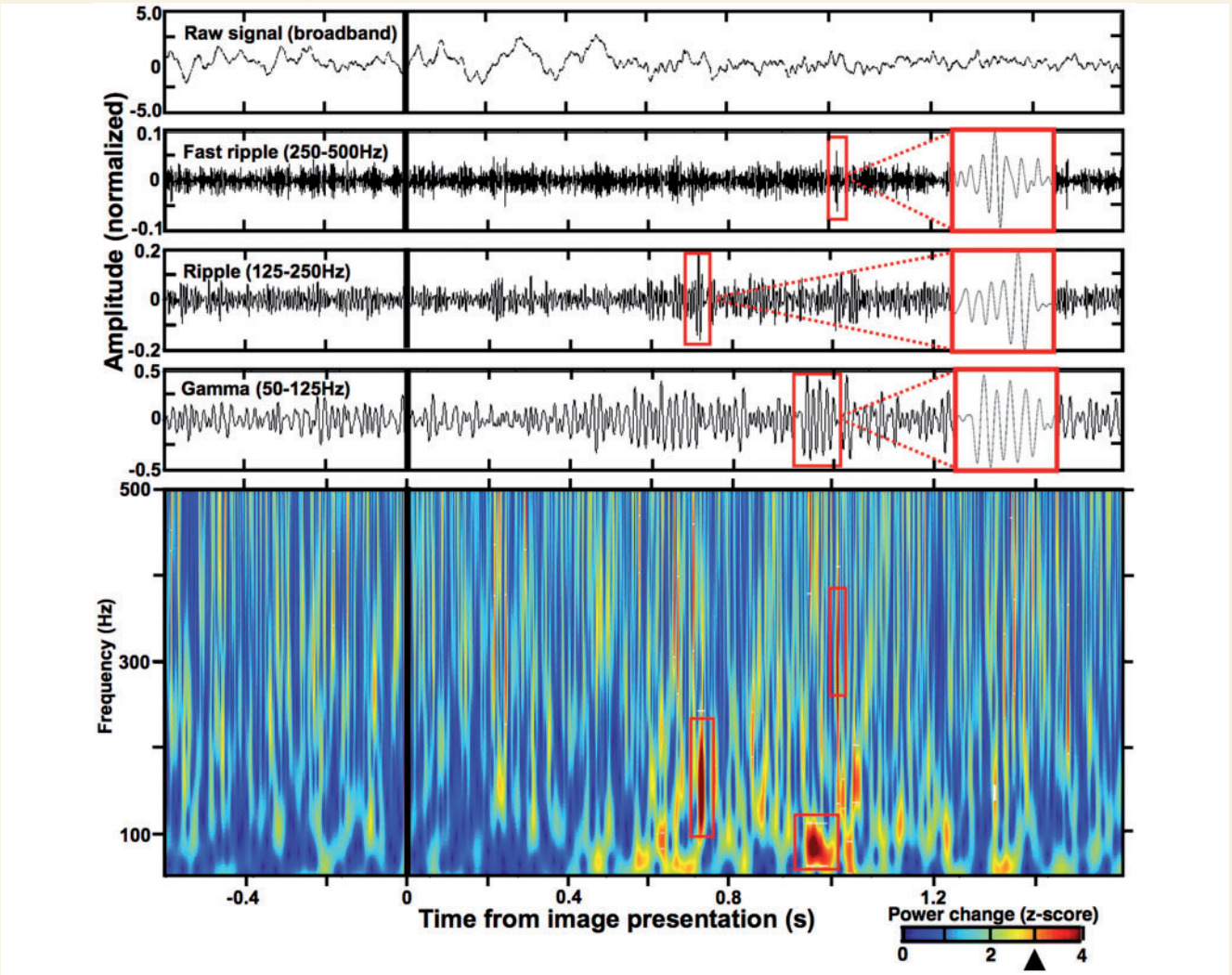

Figure 3 Detection of individual HFO discharges using Hilbert transform of filtered z-scored data. (*Top*) The upper panels show an example 2 s stretch of broadband and filtered data signal (Butterworth bandpass filters, third order) recorded from a prefrontal cortical surface electrode in Patient 7 around the time of image presentation (black vertical lines). Red rectangles correspond to the detections marked in the bottom spectrogram. (*Bottom*) Power spectrogram (50–500 Hz) of the data epoch from the *top* panel was obtained by applying Hilbert transform to 1 Hz filtered bands of z-scored signal (Canolty *et al.*, 2006; Matsumoto *et al.*, 2013*a*, *b*), calculated from 18 s of the full trial epoch from 6 s before to 12 s after image presentation (note, only 2 s are shown in this figure). Significant HFO power increases were determined at z-score = 3.0 threshold (black arrowhead on the power scale; see 'Materials and methods' section) and three representative HFO detections are highlighted by the red rectangles on the spectrogram, as well as on the corresponding filtered data signal above (close up in view in the red rectangle attached from the dashed lines). Notice that the three detections have discrete durations around specific HFO frequencies congruent with the quantification method in Fig. 2 (see Supplementary Fig. 1 for an artefact comparison). See Figs 4 and 5 for the summary of all the detected HFO properties.

The discrete HFOs were significantly longer in the hippocampus, amygdala and the parahippocampal cortex than in the other cortical regions (Fig. 4C; Wilcoxon rank sum test, $P < 0.01$). The high gamma, ripple and fast ripple HFOs revealed consistent distributions and significant differences of the detected durations across the studied regions and the task stages (Fig. 5; Wilcoxon rank sum test, $P < 0.01$). On average a gamma, ripple or fast ripple HFO event had between 4–10 cycles and the majority lasted 10–30 ms (Fig. 5)—the critical time-window for synaptic interactions between neuronal assemblies (Harris *et al.*, 2003). Furthermore, the relative proportion of gamma, ripple and fast ripple HFO detections was different across the studied structures (Fig. 4D); the ratio of gamma to fast ripple HFO distribution peaks was the highest in the occipital cortex and gradually decreased along the processing stream, i.e. the relative number of the gamma and fast ripple HFOs was more balanced in the higher associational areas. Additionally, we observed significantly more ripple and fast ripple than gamma HFOs induced in the first 100 ms after stimulus presentation (Kruskal-Wallis non-parametric ANOVA, $P = 0.002$ and $P = 0.001$ in the encoding and recall stage,

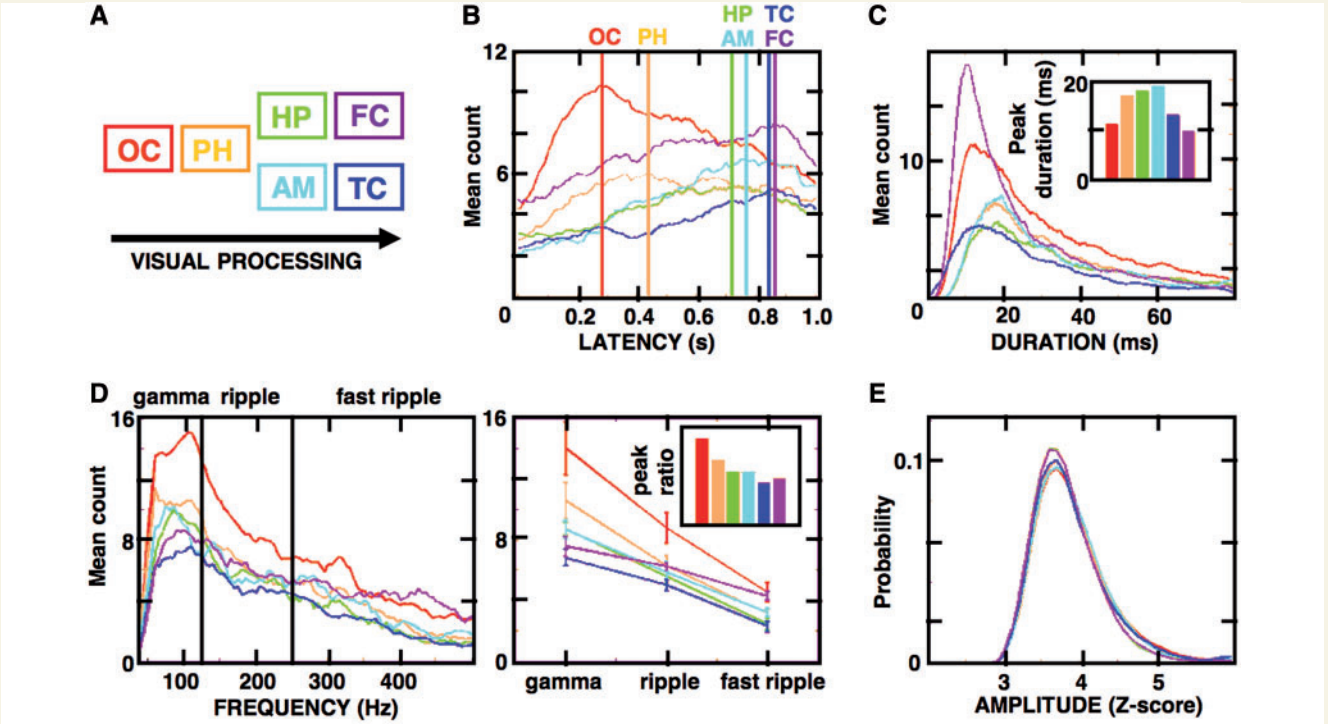

Figure 4 Induced HFOs follow the sequence of visual processing stream in the studied cortical and subcortical structures. (**A**) Diagram shows the model sequence of hypothetical visual processing stream starting in the occipital cortex (OC, red) through the parahippocampal cortex (PH, orange), hippocampus (HP, green), amygdala (AM, cyan), ending on the temporal (TC, blue) and frontal (FC, magenta) cortices. (**B–E**) These panels summarize the properties of all induced HFOs (from 0–1 s post-stimulus presentation during the encoding stage) detected on the electrodes with significant HFO responses (see Supplementary Table 1 and Fig. 2; $n = 8028$ occipital, 5294 parahippocampal, 4400 hippocampal, 2213 amygdala, 4186 temporal cortex, 3456 frontal cortex detections). (**B**) Distributions of the induced HFO latencies from image presentation (Time 0) are presented as histogram counts averaged for all electrodes in the studied structures (colour-coded vertical lines indicate the peak latency in the studied structures). Notice that the sequence of the distribution peaks follows the model processing stream (Wilcoxon rank sum test, $P < 0.01$). (**C**) Distributions of the mean HFO durations across the processing stream structures are plotted as in **B**, with values of durations corresponding to the peak HFO count summarized in the insert diagram. Notice that most HFOs in the hippocampus amygdala and parahippocampal cortex were longer than in the other cortical regions (Wilcoxon rank sum test, $P < 0.01$). (**D**, *left*) Mean HFO frequency distribution across the gamma, ripple and fast ripple bands are plotted as in **B** and **C**; (*right*) mean trial peak values from the frequency distributions are plotted for each frequency band and the gamma-to-fast ripple peak ratio is summarized in the insert diagram. Notice the differences in relative proportions of gamma and fast ripple ratios along the visual stream structures. (**E**) Mean HFO amplitudes in all structures show uniform, closely overlapping distributions. Plots in the figure were smoothed using a moving sliding average of 10 samples to facilitate data interpretation.

respectively; Fig. 5), suggesting that ripple frequency oscillations precede induced gamma HFOs. There were no significant differences between the normalized amplitudes of the detected events (Fig. 4E). Taken together, these results show that the induced HFO detections in the three studied bands have characteristic properties that parallel the hypothetical stream of cognitive processing and satisfy the temporal limits for neuronal interactions.

Induced high frequency oscillations are modulated by memory processing

To test the hypothesis that HFOs are involved in memory processing, we compared the mean HFO trial counts in the studied structures during the task encoding versus recall. There were significant differences in the trial counts for the two conditions along the sequence of the visual processing stream (Fig. 6)—encoding of images induced more HFOs than memory recall in the occipital and parahippocampal cortex (Wilcoxon rank sum test, $P = 0.002$ in both structures). On the other hand, memory recall induced significantly more HFOs than image encoding in the temporal and frontal cortex (Wilcoxon rank sum test, $P < 0.001$ in both structures). These changes are congruent with the early sensory engagement during image encoding ('bottom–up') and late associational engagement during memory recall ('top–down'; Mumford, 1992). Moreover, this pattern held and was still significant when limited to the ripple and fast ripple HFO bands (Fig. 6; Wilcoxon rank sum test, $P < 0.001$ for all four structures), meaning that memory modulation in the high frequencies is still valid when gamma HFOs were excluded from the comparison. Additionally, we observed that the latencies of HFOs induced in the temporal and frontal cortex are significantly shorter during

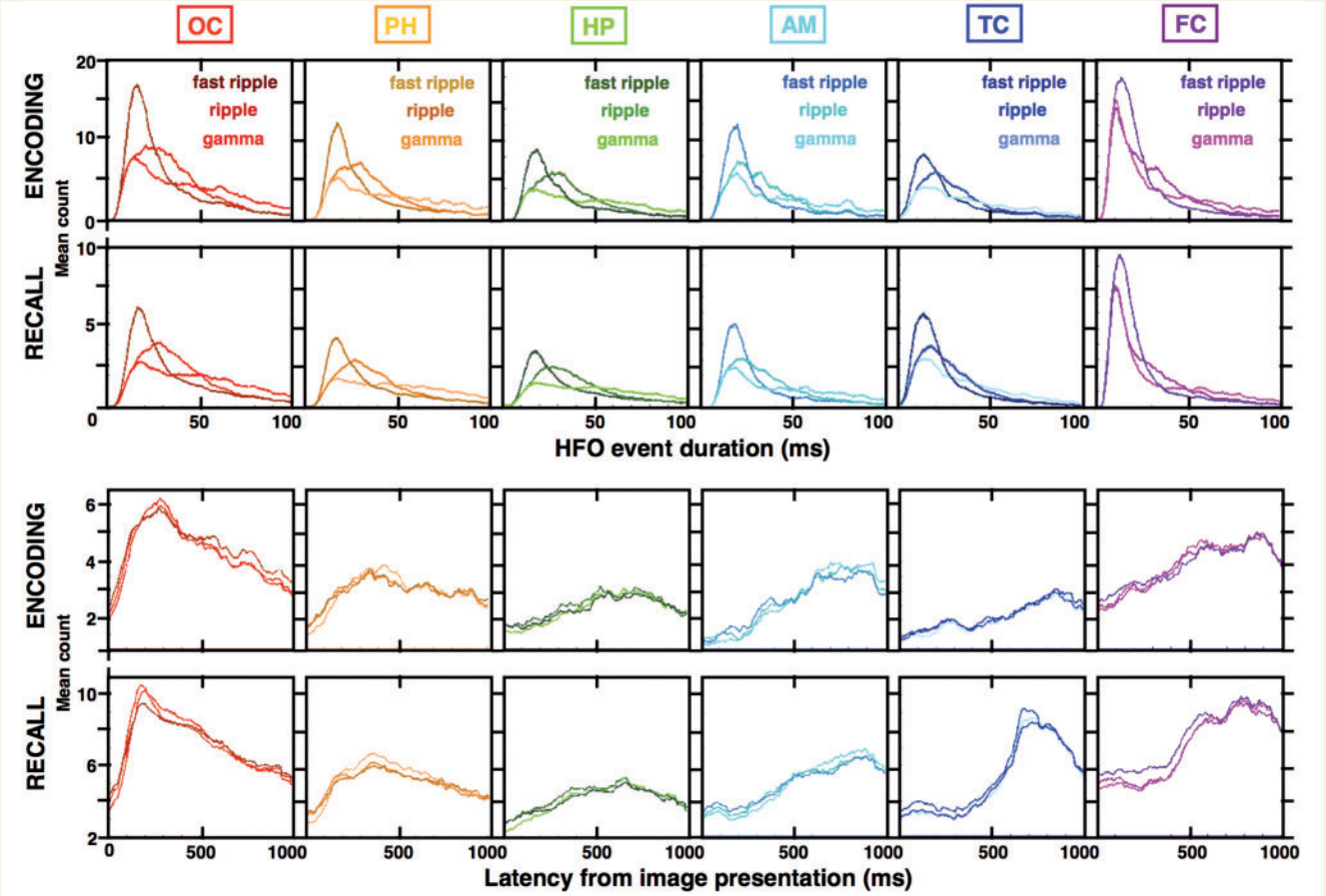

Figure 5 The high gamma, ripple and fast ripple induced HFOs have distinct durations and consistent latencies from image presentation. Distributions of all induced HFO detections from Fig. 4 (from the encoding stage of the task) were broken down into the high gamma, ripple and fast ripple bands and presented together with all the detections from the recall stage [$n = 18\,095$ occipital (OC), 13 755 parahippocampal (PH), 9317 hippocampal (HP), 4965 amygdala (AM), 7706 temporal cortex (TC), 6729 frontal cortex (FC) detections]. (**A**) Histogram counts of gamma, ripple and fast ripple HFO durations reveal distinct population distributions with significantly different means in every color-coded structure (gamma > ripple > fast ripple, Wilcoxon rank sum test, $P < 0.01$). The average HFO duration in each band corresponds to ~4–10 cycles of oscillation. (**B**) The three HFO bands show overlapping distributions of the mean latency trial counts from image presentation and show the same progression along the visual processing stream as in Fig. 4—the sharp induction of the occipital HFOs early after image presentation, followed by gradual accumulation in subsequent structures of the visual stream with late peaks in the temporal and frontal cortices. Plots in the figure were smoothed using a moving sliding average of 10 samples to facilitate data interpretation. Notice that the durations and latencies were consistent in the encoding and recall stage of the task in all structures except for temporal and frontal cortex, where HFO latencies were significantly longer during memory recall (see Fig. 6 for memory modulation of the HFO counts in the six structures during the two task stages).

memory encoding than during recall (Wilcoxon rank sum test, $P < 0.001$; see Fig. 5). No significant differences were detected in the other structures suggesting selective memory modulation of HFO induction latencies in the associational cortical areas involved in higher order visual processing.

The remaining question is whether HFOs reflect cognitive processing of particular memorized items? There is growing evidence implicating gamma oscillations in selective binding of object representations (Singer and Gray, 1995; Tallon-Baudry and Bertrand, 1999; Fries, 2009; Lachaux *et al.*, 2012) but little is known about the role of ripple and fast ripple frequencies in these cognitive processes. First of all, HFOs were significantly induced in all three bands as assessed by modulation of the mean HFO count variance (Kruskal-Wallis test, $P < 0.01$; Fig. 2) and by significant difference in the trial count before and after image presentation (Fig. 7A and B; see 'Materials and methods' section). These induced HFO responses to image presentation were found to be significantly different on the recall trials, and hence discriminate the trials with encoded images (i.e. previously seen by the subject during the encoding stage), than on the trials with novel images (not presented to the subject during the encoding stage)—the effect was significant even in the highest fast ripple frequency band (Fig. 7B; verified with Friedman ANOVA for the effect of trial type, fast ripple: $P = 0.013$, ripple: $P = 0.40$, gamma: $P = 0.65$; Bonferroni correction to $P < 0.0167$). Analogous differences were observed between the encoding trials with affectively charged

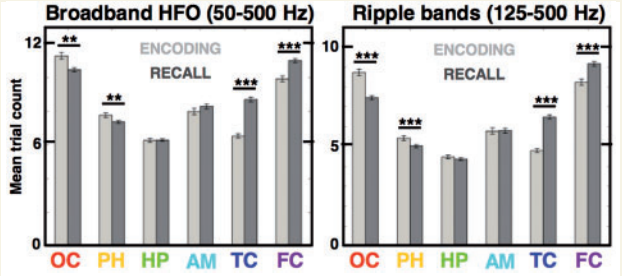

Figure 6 Human memory encoding and recall reveals bottom-up and top-down modulation of the induced HFOs. Bar plots compare mean trial counts of all induced HFOs (Fig. 4) during image encoding versus recall across the structures of the model visual processing stream. Memory encoding induced significantly more HFOs per trial in the early 'sensory' stream areas contrasted by the 'association' areas, which noted significantly more HFOs during memory recall [Wilcoxon rank sum test; $^{**}P < 0.01$, $^{***}P < 0.001$; $n = 5450$ occipital (OC), 3504 parahippocampal (PH), 2947 hippocampal (HC), 1541 amygdala (AM), 2930 temporal cortex (TC), 2659 frontal cortex (FC) detections in the encoding stage and $n = 11\,931$ occipital, 8784 parahippocampal, 6086 hippocampal, 3334 amygdala, 5545 temporal cortex, 5028 frontal cortex in the recall stage). Notice that this effect was still significant when limited to the 125–500 Hz ripple and fast ripple bands, excluding gamma HFOs (*right*).

versus neutral images, distinguishing the emotional valence of the presented images (Supplementary Fig. 4). Correct versus incorrect trials were not compared due to low number of recognition errors. There was no discernible pattern of significant HFO responses to specific images. The predictive responses to general stimulus properties that we describe (encoded versus novel and affective versus neutral) are reminiscent of selective evoked field responses to object categories, and not to specific items (Liu *et al.*, 2009). We summarized the total number of electrodes, which showed significant HFO responses, and the proportion of these that responded differentially to the encoded and to the affectively charged images in at least one of the studied HFO bands (Supplementary Table 1 and Fig. 7C). There were at least 23% of electrodes revealing discriminative HFO responses to affective charge and to memory of the presented images in every structure of the processing stream. The highest proportions of such electrodes were found in the temporal lobe structures of the hippocampus, amygdala and the temporal cortex, ranging from 60–85% of the electrodes with significantly induced HFOs (Fig. 7C).

Discussion

Cognitively-induced high frequency oscillations extend beyond the gamma frequencies

Increasing numbers of reports from the animal and human electrophysiological studies have demonstrated network oscillations in frequencies up to 600 Hz (for review see Buzsáki and Silva, 2012). In humans, fast ripple HFOs spanning 250–500 Hz were initially associated with the pathophysiology of epilepsy (Bragin *et al.*, 1999; Staba *et al.*, 2002). Fast ripples were predominantly found in the epileptogenic hippocampus, where they selectively outnumbered the ripples as quantified by fast ripple-to-ripple ratio (Staba *et al.*, 2002). Subsequent studies demonstrated that gamma (Worrell *et al.*, 2004) and ripple (Worrell *et al.*, 2008), as well as fast ripple HFOs were also increased in human epileptic brain (Worrell and Gotman, 2011). It is therefore critical for any study of physiological HFOs to control for the possible confound of pathological activities in patients with epilepsy. Here we took a conservative methodological approach to minimize this confound (see 'Materials and methods' section and Supplementary Table 1) and selected only electrodes without any evidence of epileptiform spikes, sharp waves, or seizure activity in the prolonged continuous recording. In contrast to what has been reported in epileptogenic brain (Staba *et al.*, 2002), in these selected electrodes we observed a decreasing number of induced HFOs with increasing frequencies (as in Figs 2, 6). Additionally, we have shown that the HFOs induced by image presentation in our task have significantly different properties compared to pathological HFOs, primarily, lower amplitude and shorter duration (Matsumoto *et al.*, 2013*a*). Although the possibility of the disease-related processes interfering with the reported oscillations cannot be completely ruled out in epilepsy patient recordings, the spatiotemporal profile of the HFOs induced in specific brain areas with latencies of the visual processing stream, as well as the non-pathological properties (Matsumoto *et al.*, 2013*a*), support a physiological origin.

Other studies using intracranial recordings from epilepsy patients reported physiological oscillations in the high frequency ranges during behavioural tasks. Hippocampal and rhinal cortical ripples in the 80–140 Hz were demonstrated during resting nap time of a memory consolidation task, with the latter associated with successful memory performance (Axmacher *et al.*, 2008). Another study showed power changes in distinct narrow-band frequencies from 50 to 600 Hz that were induced in a word repetition task and predicted the task stage and activation of specific brain areas (Gaona *et al.*, 2011). The reported narrow-band power changes between different task phases were shown to vary independently across distinct gamma, ripple and fast ripple frequencies—an interesting finding that received controversial interpretations from others (see response to Gaona *et al.*, 2011). Our results demonstrate cognitive induction of individual HFO events, trial-by-trial, each having discrete duration and specific frequency signature in gamma, ripple, or fast ripple range up to 600 Hz. Furthermore, ripple frequency oscillations often preceded induced gamma HFOs raising the possibility of temporal relationship between the two HFO classes.

The induced HFO events were detected by two independent spectral analysis methods: multi-taper Fast Fourier Transform analysis (Bokil *et al.*, 2010), and normalized Hilbert transform (as in Canolty *et al.*, 2006), that yielded closely overlapping patterns (Fig. 2; see Matsumoto *et al.*, 2013*b*). A similar detection approach was employed in a recent study of high gamma and ripple HFOs in rodents (Sullivan *et al.*, 2011). The authors, using a lower *z*-score threshold of 2.0 for detection, recorded

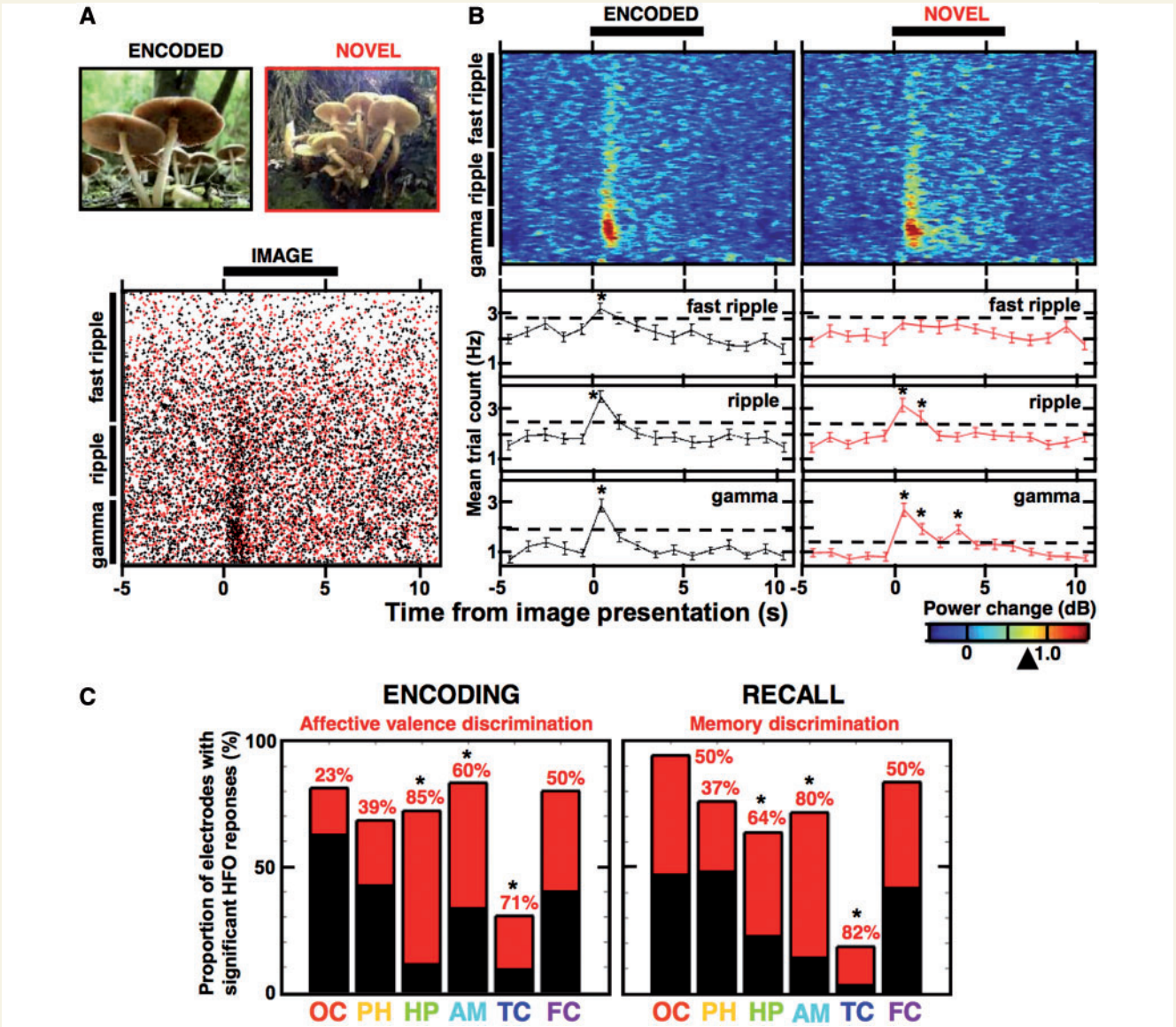

Figure 7 Induced HFOs reveal discriminative responses to the encoded images. (**A**, *top*) Examples of two similar pictures (analogous to the International Affective Picture System (IAPS) set of images used in the study, which were not allowed for publication)—one previously seen during encoding (black code) and the other novel (red code); (**A**, *bottom*) cumulative scatterplot of all HFO detections in the three frequency bands recorded from an example amygdala electrode in Patient 8 during his memory recall—black dots were detected from trials with encoded images and the red dots from trials with novel images of the same session (black bar indicates the time-course of image presentation). (**B**, *top*) Spectrograms summarize trial-averaged power changes (plotted as in Fig. 2) in the two trial types from the scatterplot in **A**, (**B**, *bottom*) the mean trial counts for the scatterplot in **A** (see Fig. 2) are summarized separately for the gamma, ripple and fast ripple detections, aligned to the trial time-course of the spectrograms. Notice significant induction of the HFOs in individual bins as compared to matched average count from the five 'baseline' bins (Wilcoxon signed-rank test, $^*P < 0.01$, encoded: 77 trials; novel: 55 trials), which is not present in the fast ripple response to novel images and was significantly different from the fast ripple response to encoded images (Friedman ANOVA, eight time bins, 55 trials, $P = 0.013$; see Fig. 2). (**C**) Proportion of all electrodes that showed discriminative HFO responses (as in **B**) to affectively charged images during encoding (*left*) and to the encoded images during recall (*right*) are summarized across the studied structures (the total black bar indicates number of electrodes with significantly induced HFOs and its red part indicates fraction of these electrodes that showed significant differences; see Supplementary Table 1). Notice that the highest fraction of electrodes with the discriminative HFO responses is reported in the hippocampus, amygdala and the temporal cortex, consistently exceeding 50% (marked with asterisk).

hippocampal sharp-wave associated events in the two frequency ranges occurring spontaneously in freely-moving rats. They reported distinct spectral and anatomical properties of the ripple and high gamma HFOs, albeit common neuronal networks and mechanisms. This finding was explained in terms of different resonant properties of networks responding to a synchronizing event like hippocampal sharp-waves. Evoked response to stimuli presentation could be the synchronizing event in case of our experiment,

given the evidence for common mechanisms underlying the evoked and induced responses (David *et al.*, 2006). In agreement with the results of Sullivan *et al.* (2011), our induced ripple HFOs were significantly shorter than high gamma events showing different distributions of durations (Fig. 5); even though, both were in general shorter than the rodent hippocampal sharp-wave ripples averaging between 10–30 ms, the HFOs detected in the medial temporal lobe structures were still significantly longer than in the neocortex (Fig. 4C).

The relationship between the cognitively-induced HFOs and the spontaneously occurring ripple oscillations in human hippocampus and neocortex remains to be established. The latter were previously described during human sleep and wakefulness (Bragin *et al.*, 1999; Staba *et al.*, 2002; Le Van Quyen *et al.*, 2010) and their neuronal mechanisms translated from the rodent studies (Le Van Quyen *et al.*, 2008). In particular, the authors of those reports have shown that, like in the case of the rodent sharp-wave ripple complexes, units coordinated their firing to specific phase of ripple HFO cycle in humans, during which interneurons fired before pyramidal cells. The neuronal correlates of induced ripples and fast ripples, or cortical HFOs remain to be explored but given the evidence from human (Le Van Quyen *et al.*, 2008, 2010) and rodent studies (Sullivan *et al.*, 2011) they could share similar networks and mechanisms.

Ripple and fast ripple frequency oscillations as a correlate of cognitive processing

Intracranial recordings from multiple cortical surface and deep brain penetrating electrodes provide a unique opportunity to sample the activity underlying cognitive processing of neuronal networks (Engel *et al.*, 2005; Jerbi *et al.*, 2009; Jacobs and Kahana, 2010; Lachaux *et al.*, 2012). Network oscillations in gamma frequencies and above were previously shown to correlate with synchronized unit firing (Baker *et al.*, 2003; Ray *et al.*, 2008; Manning *et al.*, 2009; Telenczuk *et al.*, 2011) and, in this study were induced in focal brain areas of the visual processing stream during a recognition memory task. Most of these induced oscillations lasted between 10–25 ms, which corresponds to the window for synaptic interactions of neuronal ensembles (Harris *et al.*, 2003; O'Neill *et al.*, 2008) and the time frame of gamma cycle synchronization proposed to bind perceptual and memory representations (Jensen *et al.*, 2007; Fries, 2009; Tallon-Baudry, 2009). Gamma oscillations were previously shown to correlate with memory loading, formation and maintenance (Howard *et al.*, 2003; Sederberg *et al.*, 2007; Roux *et al.*, 2012). Therefore, it is plausible that the ripple and fast ripple oscillations induced in our task, which noted significant modulation by the task memory phase even when high gamma oscillations were excluded (Fig. 6) and were found to have longer latencies during memory recall relative to encoding (Fig. 5), reflect cognitive processing of the presented images.

Unlike the highly selective responses reported in studies of single unit firing (Quiroga *et al.*, 2005), the HFO responses were not specific for individual items presented but rather discriminated more general stimulus properties—reminiscent of category-specific field potential responses to visual stimuli (Liu *et al.*, 2009). Nevertheless, the latencies of our HFOs induced in different structures of the visual processing stream are congruent with the latencies reported previously for unit firing responses to image presentations (Mormann *et al.*, 2008). Furthermore, the highest proportion of electrodes showing discriminative HFO responses was found in the medial temporal lobe structures (Fig. 7C), in agreement with the findings from previous human unit studies (Mormann *et al.*, 2008; Quian Quiroga *et al.*, 2009). All things considered, we hypothesize that the induced HFOs likely reflect coordinated activity of multiple stimulus-specific neurons responding to the presented images.

There is a growing demand for clinical biomarkers of cognitive processing in neurological and neuropsychiatric disorders. Network oscillations in the gamma and higher frequency ranges may effectively bridge the spatiotemporal resolution of the unit recordings with the larger sampling volumes used in non-invasive imaging of brain activity (Crone *et al.*, 2006; Jerbi *et al.*, 2009; Lachaux *et al.*, 2012; Silva, 2013). The spectral power of high frequency oscillations has been shown to reliably predict functional MRI signal responses (Logothetis *et al.*, 2001; Brovelli *et al.*, 2005; Niessing *et al.*, 2005) and has been shown to correlate with both functional MRI and unit firing responses to cognitive stimuli (Issa *et al.*, 2013). In the advent of new technologies developed to map the activity of the human brain, HFOs show promise as clinical biomarkers of cognitive processing in widely distributed neuronal networks in health and disease. They have been proposed to mark pathological network activity in epilepsy (Staba, 2010; Worrell and Gotman, 2011) and to indicate abnormal network synchrony underlying cognitive deficits in neuropsychiatric disorders including schizophrenia (Uhlhaas and Singer, 2012). Once the field gains a better understanding of the neuronal mechanisms of HFO, they can be especially effective in guiding the development of pharmacological or other treatments on the level of local network activity.

Acknowledgements

We would like to thank Prof. Mark Richardson for comments on the manuscript, and Cindy Nelson and Karla Crockett for their help in organizing the experiments and collecting the data. Special thanks to David Cheney for creating the patient recording illustration.

Funding

This work was supported by the National Institute of Health: R01 – NS63039 and U24 – NS063930, IGA MZCR NT/11536-5, European Regional Development Fund-Project FNUSA – ICRC (No. CZ.1.05/1.1.00/02.0123), European Social Fund and the State Budget of the Czech Republic – Project ICRC Human Bridge – Support of Study Stays of Czech Researchers Abroad III: Young Talent Incubator (CZ.1.07/2.3.00/20.0239).

Supplementary material

Supplementary material is available at *Brain* online.

References

Axmacher N, Elger CE, Fell J. Ripples in the medial temporal lobe are relevant for human memory consolidation. Brain J Neurol 2008; 131: 1806–17.

Ball T, Kern M, Mutschler I, Aertsen A, Schulze-Bonhage A. Signal quality of simultaneously recorded invasive and non-invasive EEG. Neuroimage 2009; 46: 708–16.

Baker SN, Gabriel C, Lemon RN. EEG oscillations at 600 Hz are macroscopic markers for cortical spike bursts. J Physiol 2003; 550: 529–34.

Barth DS. Submillisecond synchronization of fast electrical oscillations in neocortex. J Neurosci 2003; 23: 2502–10.

Bokil H, Andrews P, Kulkarni JE, Mehta S, Mitra PP. Chronux: a platform for analyzing neural signals. J Neurosci Methods 2010; 192: 146–51.

Bragin A, Engel J Jr, Wilson CL, Fried I, Buzsáki G. High-frequency oscillations in human brain. Hippocampus 1999; 9: 137–42.

Brinkmann BH, Bower MR, Stengel KA, Worrell GA, Stead M. Large-scale electrophysiology: acquisition, compression, encryption, and storage of big data. J Neurosci Methods 2009; 180: 185–92.

Brovelli A, Lachaux J-P, Kahane P, Boussaoud D. High gamma frequency oscillatory activity dissociates attention from intention in the human premotor cortex. Neuroimage 2005; 28: 154–64.

Burke JF, Zaghloul KA, Jacobs J, Williams RB, Sperling MR, Sharan AD, et al. Synchronous and asynchronous theta and gamma activity during episodic memory formation. J Neurosci 2013; 33: 292–304.

Buzsáki G. Rhythms of the brain. Oxford: Oxford University Press; 2006.

Buzsáki G, Horváth Z, Urioste R, Hetke J, Wise K. High-frequency network oscillation in the hippocampus. Science 1992; 256: 1025–7.

Buzsáki G, da Silva FL. High frequency oscillations in the intact brain. Prog Neurobiol 2012; 98: 241–9.

Canolty RT, Edwards E, Dalal SS, Soltani M, Nagarajan SS, Kirsch HE, et al. High gamma power is phase-locked to theta oscillations in human neocortex. Science 2006; 313: 1626–8.

Crone NE, Sinai A, Korzeniewska A. High frequency gamma oscillations and human brain mapping with electrocorticography. Prog Brain Res 2006; 159: 275–95.

Curio G. Linking 600 Hz 'spikelike' EEG/MEG wavelets ('sigma-bursts') to cellular substrates: concepts and caveats. J Clin Neurophysiol 2000; 17: 337–96.

David O, Kilner JM, Friston KJ. Mechanisms of evoked and induced responses in MEG/EEG. Neuroimage 2006; 31: 1580–91.

Dragoi G, Tonegawa S. Preplay of future place cell sequences by hippocampal cellular assemblies. Nature 2011; 469: 397–401.

Engel AK, Moll CKE, Fried I, Ojemann GA. Invasive recordings from the human brain: clinical insights and beyond. Nat Rev Neurosci 2005; 6: 35–47.

Engel J Jr. Biomarkers in epilepsy: introduction. Biomark Med 2011; 5: 537–44.

Foster DJ, Wilson MA. Reverse replay of behavioural sequences in hippocampal place cells during the awake state. Nature 2006; 440: 680–3.

Fries P. Neuronal gamma-band synchronization as a fundamental process in cortical computation. Annu Rev Neurosci 2009; 32: 209–24.

Gaona CM, Sharma M, Freudenburg ZV, Breshears JD, Bundy DT, Roland J, et al. Nonuniform high-gamma (60–500 Hz) power changes dissociate cognitive task and anatomy in human cortex. J Neurosci 2011; 31: 2091–100.

Harris KD, Csicsvari J, Hirase H, Dragoi G, Buzsáki G. Organization of cell assemblies in the hippocampus. Nature 2003; 424: 552–6.

Howard MW, Rizzuto DS, Caplan JB, Madsen JR, Lisman J, Aschenbrenner-Scheibe R, et al. Gamma oscillations correlate with working memory load in humans. Cereb Cortex 2003; 13: 1369–74.

Issa EB, Papanastassiou AM, DiCarlo JJ. Large-scale, high-resolution neurophysiological maps underlying fMRI of macaque temporal lobe. J Neurosci 2013; 33: 15207–19.

Jacobs J, Kahana MJ. Direct brain recordings fuel advances in cognitive electrophysiology. Trends Cogn Sci 2010; 14: 162–71.

Jadhav SP, Kemere C, German PW, Frank LM. Awake hippocampal sharp-wave ripples support spatial memory. Science 2012; 336: 1454–8.

Jensen O, Kaiser J, Lachaux JP. Human gamma-frequency oscillations associated with attention and memory. Trends Neurosci 2007; 30: 317–24.

Jerbi K, Ossandón T, Hamamé CM, Senova S, Dalal SS, Jung J, et al. Task-related gamma-band dynamics from an intracerebral perspective: review and implications for surface EEG and MEG. Hum Brain Mapp 2009; 30: 1758–71.

Kovach CK, Tsuchiya N, Kawasaki H, Oya H, Howard MA, Adolphs R. Manifestation of ocular-muscle EMG contamination in human intracranial recordings. Neuroimage 2011; 54: 213–33.

Lachaux JP, Axmacher N, Mormann F, Halgren E, Crone NE. High-frequency neural activity and human cognition: past, present and possible future of intracranial EEG research. Prog Neurobiol 2012; 98: 279–301.

Lang PJ, Bradley MM, Cuthbert BN. International Affective Picture System (IAPS): technical manual and affective ratings. 1997.

Le Van Quyen M. High frequency oscillations in cognition and epilepsy. Prog Neurobiol 2012; 98: 239–40.

Le Van Quyen M, Bragin A, Staba R, Crépon B, Wilson CL, Engel J Jr. Cell type-specific firing during ripple oscillations in the hippocampal formation of humans. J Neurosci 2008; 28: 6104–10.

Le Van Quyen M, Staba R, Bragin A, Dickson C, Valderama M, Fried I, et al. Large-scale micro-electrode recordings of high-frequency gamma oscillations in human cortex during sleep. J Neurosci 2010; 30: 7770–82.

Liu H, Agam Y, Madsen JR, Kreiman G. Timing, timing, timing: fast decoding of object information from intracranial field potentials in human visual cortex. Neuron 2009; 62: 281–90.

Logothetis NK, Pauls J, Augath M, Trinath T, Oeltermann A. Neurophysiological investigation of the basis of the fMRI signal. Nature 2001; 412: 150–7.

Manning JR, Jacobs J, Fried I, Kahana MJ. Broadband shifts in local field potential power spectra are correlated with single-neuron spiking in humans. J Neurosci 2009; 29: 13613–20.

Matsumoto A, Brinkmann BH, Stead SM, Matsumoto J, Kucewicz M, Marsh WR, et al. Pathological and physiological high frequency oscillations in focal human epilepsy. J Neurophysiol 2013a; 110: 1958–64.

Matsumoto JY, Stead M, Kucewicz MT, Matsumoto AJ, Peters PA, Brinkmann BH, et al. Network oscillations modulate interictal epileptiform spike rate during human memory. Brain 2013b; 136: 2444–56.

Mishkin M, Ungerleider LG, Macko KA. Object vision and spatial vision: two cortical pathways. Trends Neurosci 1983; 6: 414–7.

Mormann F, Kornblith S, Quiroga RQ, Kraskov A, Cerf M, Fried I, et al. Latency and selectivity of single neurons indicate hierarchical processing in the human medial temporal lobe. J Neurosci 2008; 28: 8865–72.

Mumford D. On the computational architecture of the neocortex. Biol Cybern 1992; 66: 241–51.

Niessing J, Ebisch B, Schmidt KE, Niessing M, Singer W, Galuske RA. Hemodynamic signals correlate tightly with synchronized gamma oscillations. Science 2005; 309: 948–51.

O'Neill J, Senior TJ, Allen K, Huxter JR, Csicsvari J. Reactivation of experience-dependent cell assembly patterns in the hippocampus. Nat Neurosci 2008; 11: 209–15.

Quian Quiroga R, Kraskov A, Koch C, Fried I. Explicit encoding of multimodal percepts by single neurons in the human brain. Curr Biol 2009; 19: 1308–13.

Quiroga RQ, Reddy L, Kreiman G, Koch C, Fried I. Invariant visual representation by single neurons in the human brain. Nature 2005; 435: 1102–7.

Ray S, Crone NE, Niebur E, Franaszczuk PJ, Hsiao SS. Neural correlates of high-gamma oscillations (60-200 Hz) in macaque local field potentials and their potential implications in electrocorticography. J Neurosci 2008; 28: 11526–36.

Roux F, Wibral M, Mohr HM, Singer W, Uhlhaas PJ. Gamma-band activity in human prefrontal cortex codes for the number of relevant items maintained in working memory. J Neurosci 2012; 32: 12411–20.

Sederberg PB, Schulze-Bonhage A, Madsen JR, Bromfield EB, McCarthy DC, Brandt A, et al. Hippocampal and neocortical gamma oscillations predict memory formation in humans. Cereb Cortex 2007; 17: 1190–6.

Silva FL. EEG and MEG: relevance to neuroscience. Neuron 2013; 80: 1112–28.

Singer AC, Carr MF, Karlsson MP, Frank LM. Hippocampal SWR activity predicts correct decisions during the initial learning of an alternation task. Neuron 2013; 77: 1163–73.

Singer W, Gray CM. Visual feature integration and the temporal correlation hypothesis. Annu Rev Neurosci 1995; 18: 555–86.

Staba RJ. Normal and pathologic high-frequency oscillations. Epilepsia 2010; 51: 21.

Staba RJ, Wilson CL, Bragin A, Fried I, Engel J Jr. Quantitative analysis of high-frequency oscillations (80–500 Hz) recorded in human epileptic hippocampus and entorhinal cortex. J Neurophysiol 2002; 88: 1743–52.

Sullivan D, Csicsvari J, Mizuseki K, Montgomery S, Diba K, Buzsaki G. Relationships between hippocampal sharp waves, ripples and fast gamma oscillation: influence of dentate and entorhinal cortical activity. J Neurosci 2011; 31: 8605–16.

Tallon-Baudry C. The roles of gamma-band oscillatory synchrony in human visual cognition. Front Biosci (Landmark Ed) 2009; 14: 321–32.

Tallon-Baudry C, Bertrand O. Oscillatory gamma activity in humans and its role in object representation. Trends Cogn Sci 1999; 3: 151–62.

Telenczuk B, Baker SN, Herz AVM, Curio G. High-frequency EEG covaries with spike burst patterns detected in cortical neurons. J Neurophysiol 2011; 105: 2951–9.

Traub RD, Whittington MA. Cortical oscillations in health and disease. Oxford University Press; 2010.

Uhlhaas PJ, Singer W. Neuronal dynamics and neuropsychiatric disorders: toward a translational paradigm for dysfunctional large-scale networks. Neuron 2012; 75: 963–80.

Van Vugt MK, Sederberg PB, Kahana MJ. Comparison of spectral analysis methods for characterizing brain oscillations. J Neurosci Methods 2007; 162: 49–63.

Wilson MA, McNaughton BL. Recativation of hippocampal ensemble memories during sleep. Science 1994; 265: 676–9.

Worrell GA, Gardner AB, Stead SM, Hu S, Goerss S, Cascino GJ, et al. High-frequency oscillations in human temporal lobe: simultaneous microwire and clinical macro-electrode recordings. Brain 2008; 131: 928–37.

Worrell G, Gotman J. High-frequency oscillations and other electrophysiological biomarkers of epilepsy: clinical studies. Biomark Med 2011; 5: 557–66.

Worrell GA, Jerbi K, Kobayashi K, Lina JM, Zelmann R, Le Van Quyen M. Recording and analysis techniques for high-frequency oscillations. Prog Neurobiol 2012; 98: 265–278.

Worrell GA, Parish L, Cranstoun SD, Jonas R, Baltuch G, Litt B. High-frequency oscillations and seizure generation in neocortical epilepsy. Brain 2004; 127: 1496–506.

Yuval-Greenberg S, Tomer O, Keren AS, Nelken I, Deouell LY. Transient induced gamma-band response in EEG as a manifestation of miniature saccades. Neuron 2008; 58: 429–41.